Received: 3 July 2022 | Revised: 3 August 2022 | Accepted: 8 August 2022

DOI: 10.1002/bkcs.12608

ARTICLE

BKCS BULLETIN OF THE KOREAN CHEMICAL SOCIETY

Synthesis of monolayer 2D MoS_2 quantum dots and nanomesh films by inorganic molecular chemical vapor deposition for quantum confinement effect control

Chaehyeon Ahn | **Hyunseob Lim**

Department of Chemistry, Gwangju Institute of Science and Technology (GIST), Gwangju, Republic of Korea

Correspondence
Hyunseob Lim, Department of Chemistry, Gwangju Institute of Science and Technology (GIST), Gwangju 61005, Republic of Korea.
Email: hslim17@gist.ac.kr

Funding information
Ministry of Land, Infrastructure and Transport of Korea, Grant/Award Number: 22CTAP-C163795-02; National Research Foundation of Korea, Grant/Award Numbers: NRF-2020M3D1A1110566, NRF-2021R1A4A1027480, NRF-2021R1C1C1010603

Abstract

Bandgap engineering is an important prerequisite for various applications of two-dimensional (2D) transition metal dichalcogenides (TMD). A reduction in the dimension from 2D has been one of the methods to control the electronic structure, by which a quantum confinement effect in the additional axis(es) can result in the widening of band structures. A vapor-phase process for synthesizing monolayer MoS_2 nanomesh film or MoS_2 quantum dot is developed based on the inorganic molecular chemical vapor deposition. The vapor-phase process can control MoS_2 coverage by adjusting growth times. Therefore, the formation of nanostructures can be confirmed based on the growth time. The quantum confinement effect in monolayer MoS_2 nanomesh films and MoS_2 quantum dots is also confirmed via spectroscopic investigations, which induce a blue shift, indicating bandgap widening. Consequently, this approach can be used to synthesize lower-dimensional TMD materials for bandgap engineering, which is an essential process in optical or optoelectrical applications.

KEYWORDS
inorganic molecular chemical vapor deposition, MoS_2, nanomesh, quantum confinement effect, quantum dot

INTRODUCTION

Since the discovery of graphene opened a new era of two-dimensional (2D) materials, vigorous research on various 2D materials has revealed their intriguing characteristics, which are often distinct from the bulk structure.[1–3] In particular, extraordinary and outstanding optical properties have been confirmed in monolayer 2D materials. For example, monolayer molybdenum disulfide (MoS_2), one of the transition metal dichalcogenides (TMD) family, exhibits strong photoluminescence (PL) with an ultrahigh quantum yield owing to its direct bandgap of ~1.86, which is unlike the indirect bandgap of thicker layered MoS_2 or bulk MoS_2.[4,5] To incorporate TMD materials into conventional optoelectronic applications such as light-emitting diodes, imaging, and photocatalysts, bandgap engineering is required for tunable spectral responses.[6–8] Various approaches have been adopted for this purpose, such as alloying TMD materials (e.g., $MoS_xSe_{(2-x)}$, $Mo_xW_{(1-x)}S_2$),[9] covalent surface modification,[10] and reduction in the dimensions from 2D to 1D or 0D.[11,12]

Quantum confinement is a well-known physical effect in which low-dimensional materials have a widened bandgap when their size is smaller than the Bohr radius of the structure. Although monolayer 2D materials have their own band structures, the band structure can be modified when the lateral dimension becomes small enough to cause additional lateral quantum confinement. In the case of graphene, 1D graphene derivatives such as graphene nanoribbon,[13] graphene nanomesh,[14] and graphene nanowrinkle,[15] and 0D graphene derivative quantum dot[16] have the opened bandgap in contrast to the intrinsic zero bandgap of graphene. Following a similar approach, MoS_2 quantum dots have been evaluated as significant materials owing to their unique characteristics induced by strong quantum confinement and their numerous edge sites exhibiting highly active catalytic ability.[12,17] However, most of the developed synthetic

methods for MoS_2 quantum dots are based on the liquid-phase process,[18–20] which limits the production of monolayer MoS_2 and results in multilayer or aggregated MoS_2.

Herein, we demonstrate a unique approach to control the dimensions of monolayer 2D MoS_2 films.[21] Inorganic molecular chemical vapor deposition (IMCVD) method facilitates the high-quality MoS_2 film but with small grain size. The control of growth time unveils that monolayer MoS_2 quantum dots, which are several tens of nanometers in size, continuously merge into a monolayer MoS_2 film through the MoS_2 nanomesh structure. Spectroscopic investigations of 1D MoS_2 nanomesh and 0D MoS_2 quantum dot films reveal a widened optical bandgap owing to the lower dimensional quantum confinement effect with respect to their geometrical structures.

EXPERIMENTAL

Sample preparation

An IMCVD method, in which the entire precursor could flow in the gas state, was applied to synthesize MoS_2. Carrier gases composed of argon (99.999%, Ar) and hydrogen (99.9999%, H_2) and the sulfur precursor, hydrogen sulfide (99.5%, H_2S), were regulated using mass flow controllers. $MoOCl_4$ (Sigma-Aldrich), used as the Mo precursor, was converted into its gaseous state by heating a cylinder containing the precursor to 160 °C. First, a quartz substrate was washed with distilled water and placed in the middle of a tube furnace. Prior to the growth of MoS_2, the furnace temperature was raised to 900 °C for 1 h to clean the surface of the substrate. After the annealing process, the furnace temperature was lowered to 650 °C and we synthesized MoS_2 nanostructures at low partial-pressure conditions by flowing Ar (96 sccm), H_2 (4 sccm), H_2S (0.5 sccm), and $MoOCl_4$ ($\sim 1 \times 10^{-3}$). The optimal growth time for the MoS_2 film was 15 min, although MoS_2 nanostructures, such as nanomesh and quantum dots, could be acquired when the growth time was less than 15 min.

The as-grown MoS_2 was then transferred to the target substrate for analysis. First, polystyrene (PS) was spin-coated (4000 rpm) onto an MoS_2/quartz substrate. The PS-coated MoS_2 was then separated from the substrate by immersion in a 1.5 M KOH solution, after which it was transferred onto the target substrates. After the sample was sufficiently dried, PS was removed using toluene. The annealing process was then performed at 300 °C for 1 h to eliminate organic residues.

MICROSCOPIC CHARACTERIZATION OF SAMPLES

The investigation of the MoS_2 coverage was carried out using atomic force microscopy (AFM, SPA 500, Seiko Instrument), scanning electron microscopy (SEM, Verious5 UC, Thermal Fisher Scientific), and transmission electron microscopy (TEM, JEM-2100, JEOL). AFM analysis of MoS_2 was performed on a quartz substrate, and SEM analysis was performed on a SiO_2/Si substrate. Additionally, a 2-nm carbon film-coated TEM grid was used in the TEM analysis of the MoS_2 nanostructure to maintain the morphology grown on the substrate. Entire TEM images were measured at an acceleration voltage of 200 kV.

Spectroscopic characterization of samples

The optical properties and blue-shift tendencies caused by the quantum confinement effect, as a function of the coverage, were investigated using UV–vis spectroscopy (Agilent 8453, Agilent Technologies), Raman/PL spectroscopy, and x-ay photoelectron spectroscopy (XPS, NEXSA, Thermo Fisher Scientific). The Raman/PL spectra were acquired using a lab-designed Raman/PL spectroscopy system combined with a 532-nm laser and a ×100 magnification objective lens.

RESULTS AND DISCUSSION

Monolayer 2D MoS_2 quantum dots and nanomesh films were synthesized via IMCVD process reported in our previous literatures.[21,22] In brief, $MoOCl_4$ and H_2S were used as inorganic molecular precursors instead of solid-phase precursors like MoO_3 and S powder, which are normally used for conventional CVD processes adopted for MoS_2 growth (Figure 1a). Because the partial vapor pressure of precursors can be precisely controlled during the IMCVD process, the growth of MoS_2 is highly reproducible. The growth of MoS_2 is saturated as a monolayer even after the growth time for fully covered MoS_2 (*f*-MoS_2) grown at (t_0). The monolayer MoS_2 film was characterized using spectroscopic methods. In the Raman spectrum of the MoS_2 film (Figure 1b), the distinctive Raman modes of MoS_2 assigned to E_{2g} and A_{1g} (should it be italic), which are represented as in-plane and out-of-plane modes, can be observed at 382 and 402 cm^{-1}, respectively. The distance value between two Raman modes, $\Delta\nu \approx 20\,cm^{-1}$, presents evidence on the synthesis of MoS_2 with a monolayer thickness. In the XPS spectrum shown in Figure 1c, to confirm the atomic composition of the MoS_2 monolayer, Mo 3d peaks can be observed at 232.9 eV ($3d_{3/2}$) and 229.8 eV ($3d_{5/2}$), and S 2p peaks can be observed at 163.8 eV ($2p_{3/2}$) and 162.6 eV ($2p_{1/2}$), which are associated with the Mo^{4+} and S^{2-} states, respectively. These results are not only consistent with previously reported data on MoS_2 monolayer but also indicate that MoS_2 was synthesized with crystallinity.[23] SEM image of the MoS_2 film (Figure 1d) shows the surface morphology, in which the wrinkled structures are confirmed. Although the high crystallinity of the MoS_2 film on the quartz substrate by IMCVD was confirmed by spectroscopic characterizations, the grain size of MoS_2 was limited to several tens of

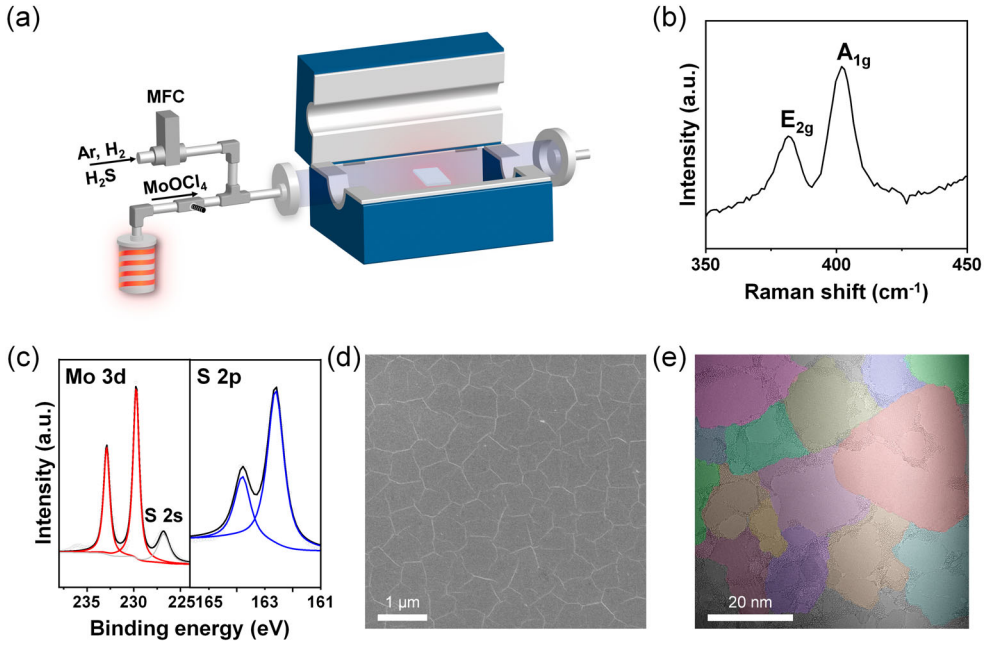

FIGURE 1 Growth method and characterization of *f*-MoS_2 via IMCVD method. (a) Scheme of the IMCVD process for MoS_2 growth. (b) Raman spectrum and (c) XPS spectra measured for the *f*-MoS_2 film. (d) SEM image of *f*-MoS_2. (e) HR-TEM image of *f*-MoS_2 represented with MoS_2 grains with different orientations

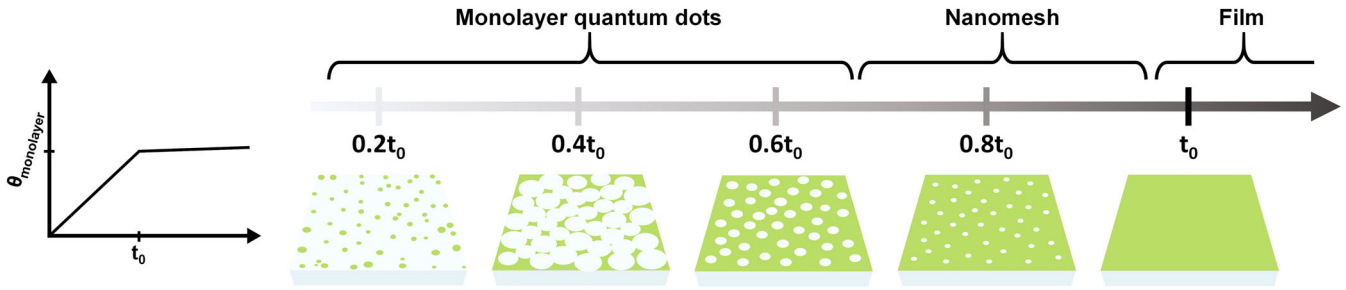

SCHEME 1 Synthesis of the MoS_2 nanostructure of the nanomesh and quantum dots depending on the growth time

nanometers, as confirmed by high-resolution transmission electron microscope (HR-TEM) image (Figure 1e). However, the small grain size obtained via IMCVD is expected to be useful for synthesizing monolayer MoS_2 quantum dots or MoS_2 nanomesh film. We expect that MoS_2 quantum dots can be formed at the initial growth state, after which the MoS_2 nanomesh can be produced before the growth of the *f*-MoS_2 film, as shown in Scheme 1.

Synthesis of monolayer MoS_2 nanomesh and MoS_2 quantum dot

According to the hypothesis suggested shown in Scheme 1, we attempted IMCVD for growth times shorter than t_0. UV–vis spectra presented in Figure 2 were obtained from the sample by increasing the growth time, and the coverage of the sample (θ) was evaluated by considering the intensity ratio of the peak of C exciton with

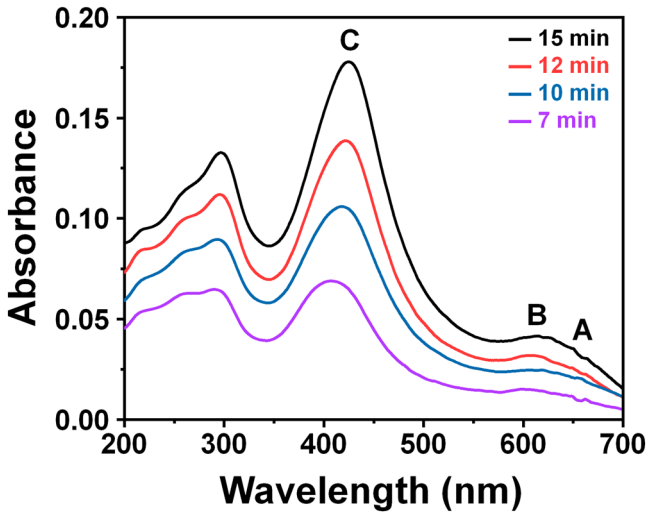

FIGURE 2 UV–vis spectra of MoS_2 acquired at different growth times

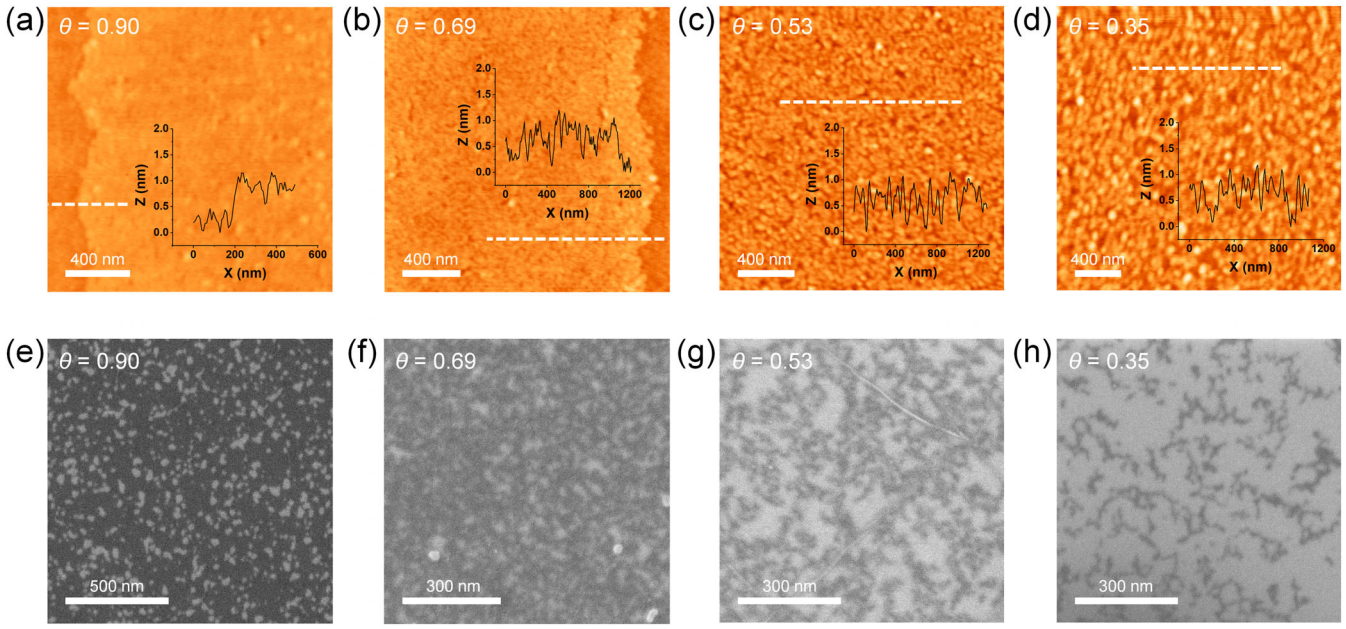

FIGURE 3 Analysis of the surface morphology. (a–d) AFM images of MoS_2 nanostructures with different coverages (θ): (a) $\theta = 0.90$, (b) $\theta = 0.69$, (c) $\theta = 0.53$, (d) $\theta = 0.35$. (e–h) SEM images of the MoS_2 samples with different coverages (θ): (e) $\theta = 0.90$, (f) $\theta = 0.69$, (g) $\theta = 0.53$, (h) $\theta = 0.35$

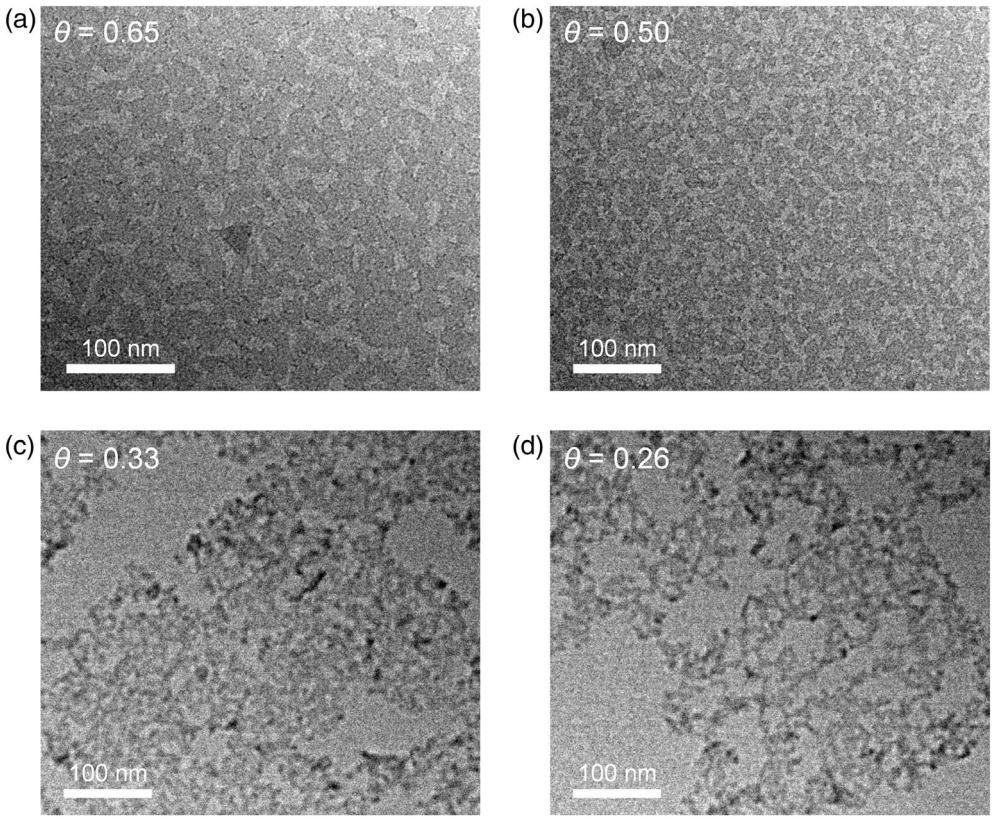

FIGURE 4 Analysis of grain distribution in MoS_2 grains. (a–d) TEM images of the MoS_2 nanostructures with different coverages (θ): (a) $\theta = 0.65$, (b) $\theta = 0.50$, (c) $\theta = 0.33$, (d) $\theta = 0.26$

respect to that of the monolayer *f*-MoS_2 ($\theta = I_C$ (sample)/I_C (*f*-MoS_2AFM)) analysis was then carried out to examine the surface morphology of the samples as a function of the growth time (Figure 3a–d). While an atomically smooth surface can be confirmed in the AFM image of nearly *f*-MoS_2 (Figure 3a), roughened surfaces can be observed for samples with θ = 0.69, 0.53, and 0.35 (Figure 3b–d) due to the presence of empty sites on the

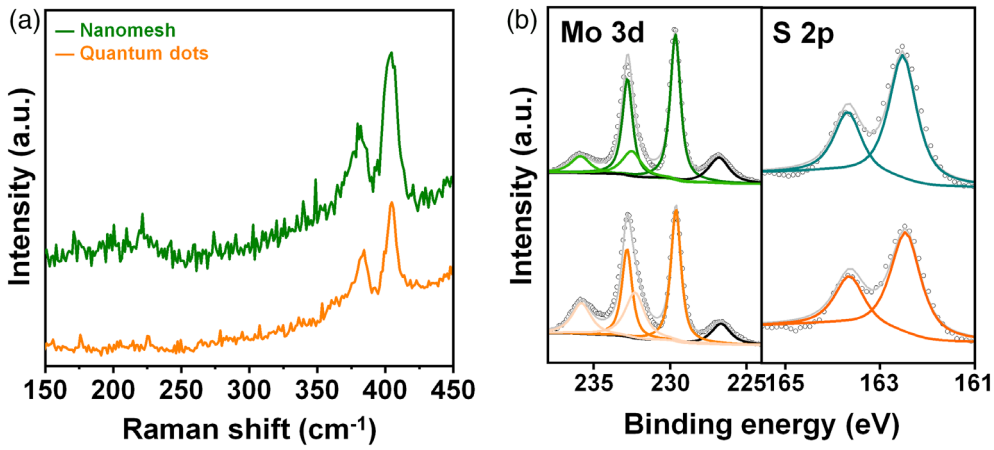

FIGURE 5 Optical characterization of the MoS_2 nanomesh film and MoS_2 quantum dots. (a) Raman spectra and (b) XPS spectra of MoS_2 nanomesh film (green) and MoS_2 quantum dots (orange)

films. Nevertheless, the height distribution confirmed in (Figure 3b–d) is in the range of 0–1 nm, which implies that the synthesized MoS_2 films consist of monolayer MoS_2.

HR-SEM images were also obtained for the samples, and they reveal the lateral shapes of the samples more clearly (Figure 3e–h). The sample with $\theta = 0.90$ presents a lower number of empty sites in the monolayer film (Figure 3e), but a sample with a lower θ ($\theta = 0.69$) exhibits a relatively higher number of empty sites (Figure 3f). Based on the lateral geometric structure of the sample, we define this state as monolayer MoS_2 nanomesh. Figure 3g,h show the SEM images of MoS_2 films with the much lower θ values of $\theta = 0.53$ and 0.35, respectively. As can be observed, they exhibit aggregations of 0D MoS_2 with sizes of several tens of nanometers but with different populations. Thus, we define these structures as monolayer MoS_2 quantum dots.

Furthermore, TEM images were obtained by transferring the samples onto a TEM grid (Figure 4). Based on the results, it can be confirmed that the grain size can be decreased continuously up to 10–20 nm by lowering the coverage from $\theta = 0.65$ (Figure 4a) to $\theta = 0.5$ (Figure 4b). Following this, the population of MoS_2 decreases from $\theta = 0.33$ (Figure 4c) to $\theta = 0.26$ (Figure 4d) with a consistent grain size of 10–20 nm.

The width of MoS_2 nanomesh and the size of quantum dots were confirmed as 10–20 nm in the TEM images (Figure 4). Therefore, growth time-dependent microscopic studies demonstrate that the IMCVD process enables a precise control of MoS_2 coverage, which facilitates the synthesis of monolayer MoS_2 nanomesh and MoS_2 quantum dot films.

Spectroscopy investigation of MoS_2 nanomesh and MoS_2 quantum dot

Raman and XPS spectroscopy were performed to investigate the chemical quality of the monolayer MoS_2 nanomesh and MoS_2 quantum dot films (Figure 5). In the Raman spectra of the MoS_2 nanomesh (green) and quantum dot (orange) (Figure 5a), distinctive Raman modes of MoS_2 assigned to E_{2g} and A_{1g} appear, which correspond to the in-plane and out-of-plane modes, respectively. Despite the small grain size of the MoS_2 nanomesh and MoS_2 quantum dot, the peak positions of the E_{2g} and A_{1g} modes and the intensity ratio between two phonon modes were almost the same as those measured for the *f*-MoS_2 film (Figure 1b). In addition, a negligible intensity of the LA mode was observed in the Raman spectra, which could be attributed to the inelastic scattering process, indicating the existence of defect in MoS_2. These Raman characteristics therefore indicate the outstanding crystallinity of the MoS_2 nanomesh and MoS_2 quantum dots, even with small grain size. In the XPS spectra measured on the monolayer MoS_2 nanomesh or quantum dots, Mo 3d peaks and S 2p peaks can be observed at 232.8 eV (Mo $3d_{3/2}$), 229.6 eV (Mo $3d_{5/2}$), 163.7 eV (S $2p_{3/2}$), and 162.5 eV (S $2p_{1/2}$) (Figure 5b). The similar peak positions of the *f*-MoS_2 film indicate the presence of Mo^{4+} and S^{2-} oxidation states. However, the Mo 3d peaks corresponding to Mo^{6+} appeared at higher binding energies than Mo^{4+} peaks. The intensity of the Mo^{6+} XPS peaks of the MoS_2 quantum dots (orange) was higher than that of the MoS_2 nanomesh (green). The appearance of Mo^{6+} peaks could be attributed to the higher number of edge sites. It is worth noting that Mo at the edge can have a Mo^{6+} oxidation state instead of a Mo^{4+} oxidation state.[24]

Nanometer-scale dimensions of the monolayer MoS_2 nanomesh and MoS_2 quantum dot films would result in a quantum confinement effect, which would widen the bandgap. To investigate this effect in detail, we measured the UV–vis and PL spectra for an increased number of samples (Figure 6). The peaks observed at ~420 nm in the UV–vis spectra can be attributed to the generation of C excitons of MoS_2, and the weak peaks observed at ~600 and ~650 nm indicate the generation of B and A

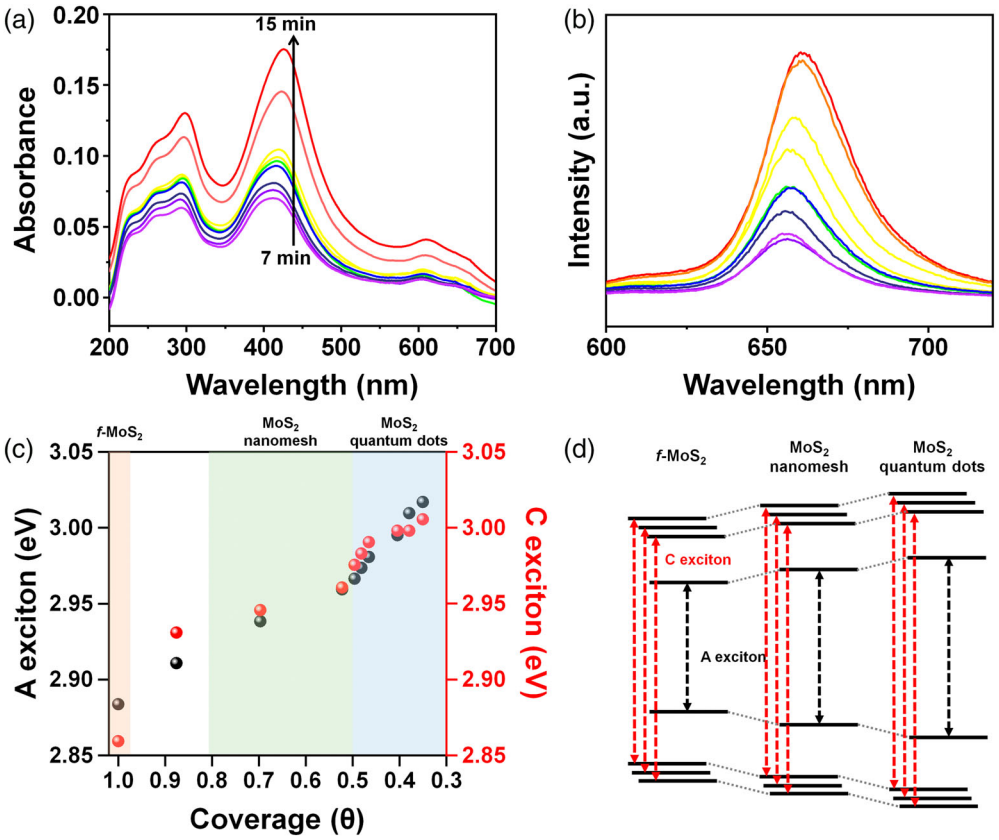

FIGURE 6 Investigation of the quantum confinement effect depending on the coverage. (a) UV–vis spectra and corresponding (b) PL spectra of MoS_2 with different coverages. (c) Coverage-dependent energy change of A and C excitons extracted from UV–vis (A) and PL (C) spectra. (d) Scheme of band widening by the quantum confinement effect in MoS_2 nanomesh and quantum dots

excitons of MoS_2 (Figure 6a). The peaks observed in the PL spectra originate from the recombination of the A exciton (Figure 6b). The peak positions of the C exciton in the UV–vis spectra and the A exciton in the PL spectra are plotted as a function of θ in Figure 6c. The blue-shift resulting from decreasing θ is confirmed for both the C and A excitons, which strongly suggests the presence of the quantum confinement effect in the monolayer MoS2 nanomesh and MoS2 quantum dot films. Because monolayer MoS2 has a direct band gap, a recombination of the A exciton corresponds to the transition from the conduction band minimum (CBM) to the valence band maximum (VBM). Thus, the blue shift of the A exciton peak in the PL spectra implies bandgap widening in the samples. Because C excitons can be generated by a transition from a deeper valence state to a higher conduction state, the simultaneously observed blue-shift of the C exciton implies entire electronic structure change for the conduction band and valence band, as well as the positions of the CBM and VBM, as illustrated in Figure 6d.

CONCLUSION

In summary, a novel chemical route to synthesize monolayer MoS_2 nanomesh and MoS_2 quantum dot films was developed using IMCVD. Since precise vapor pressure control is available in IMCVD owing to the molecular characteristics of precursors, the coverage of MoS_2 could be controlled, which facilitated the formation of monolayer MoS_2 nanomesh and MoS_2 quantum dot films on the substrate in our approach. The quantum confinement effect inducing that induced widening of the bandgap in the electronic structure was confirmed in the monolayer MoS_2 nanomesh and MoS_2 quantum dots. This indicates that the synthetic method developed in this study can be widely used for bandgap engineering of the various TMD materials required for optical or optoelectrical applications. Furthermore, we believe that our approach can also prove to be useful for developing TMD-based electrochemical catalysts because a higher degree of chemically active edge sites can be created in high-quality lower dimensional (0D or 1D) TMD materials.

ACKNOWLEDGMENTS

This work was financially supported by the National Research Foundation of Korea (NRF) (grant nos. NRF-2021 R1C1C1010603, NRF-2021R1A4A1027480, and NRF-2020 M3D1A1110566) and by the Ministry of Land, Infrastructure and Transport of Korea (22CTAP-C163795-02).

ORCID

Chaehyeon Ahn https://orcid.org/0000-0003-3515-351X
Hyunseob Lim https://orcid.org/0000-0002-4956-4208

REFERENCES

[1] Y. Zhang, Y.-W. Tan, H. L. Stormer, P. Kim, *Nature* **2005**, *438*, 201.
[2] B. Radisavljevic, A. Radenovic, J. Brivio, V. Giacometti, A. Kis, *Nat. Nanotechnol.* **2011**, *6*, 147.
[3] C. Xie, C. Mak, X. Tao, F. Yan, *Adv. Funct. Mater.* **2017**, *27*, 1603886.
[4] K. F. Mak, C. Lee, J. Hone, J. Shan, T. F. Heinz, *Phys. Rev. Lett.* **2010**, *105*, 136805.
[5] A. Splendiani, L. Sun, Y. Zhang, T. Li, J. Kim, C.-Y. Chim, G. Galli, F. Wang, *Nano Lett.* **2010**, *10*, 1271.
[6] C. Kim, T. P. Nguyen, Q. V. Le, J. M. Jeon, H. W. Jang, S. Y. Kim, *Adv. Funct. Mater.* **2015**, *25*, 4512.
[7] D. Li, W. Xiong, L. Jiang, Z. Xiao, H. Rabiee Golgir, M. Wang, X. Huang, Y. Zhou, Z. Lin, J. Song, S. Ducharme, L. Jiang, J.-F. Silvain, Y. Lu, *ACS Nano* **2016**, *10*, 3766.
[8] Q. Lu, Y. Yu, Q. Ma, B. Chen, H. Zhang, *Adv. Mater.* **2016**, *28*, 1917.
[9] C. Shang, B. Xu, X. Lei, S. Yu, D. Chen, M. Wu, B. Sun, G. Liu, C. Ouyang, *Phys. Chem. Chem. Phys.* **2018**, *20*, 20919.
[10] Y. Park, S. Shin, Y. An, J.-G. Ahn, G. Shin, C. Ahn, J. Bang, J. Baik, Y. Kim, J. Jung, H. Lim, *ACS Appl. Mater. Interfaces* **2020**, *12*, 40870.
[11] Y. Li, Z. Zhou, S. Zhang, Z. Chen, *J. Am. Chem. Soc.* **2008**, *130*, 16739.
[12] Z. Gan, L. Liu, H. Wu, Y. Hao, Y. Shan, X. Wu, P. K. Chu, *Appl. Phys. Lett.* **2015**, *106*, 233113.
[13] M. Y. Han, B. Özyilmaz, Y. Zhang, P. Kim, *Phys. Rev. Lett.* **2007**, *98*, 206805.
[14] J. Bai, X. Zhong, S. Jiang, Y. Huang, X. Duan, *Nat. Nanotechnol.* **2010**, *5*, 190.
[15] H. Lim, J. Jung, R. S. Ruoff, Y. Kim, *Nat. Commun.* **2015**, *6*, 1.
[16] S. H. Jin, D. H. Kim, G. H. Jun, S. H. Hong, S. Jeon, *ACS Nano* **2013**, *7*, 1239.
[17] T. F. Jaramillo, K. P. Jørgensen, J. Bonde, J. H. Nielsen, S. Horch, I. Chorkendorff, *Science* **2007**, *317*, 100.
[18] W. Qiao, S. Yan, X. Song, X. Zhang, Y. Sun, X. Chen, W. Zhong, Y. Du, *RSC Adv.* **2015**, *5*, 97696.
[19] W. Dai, H. Dong, B. Fugetsu, Y. Cao, H. Lu, X. Ma, X. Zhang, *Small* **2015**, *11*, 4158.
[20] X. Ren, L. Pang, Y. Zhang, X. Ren, H. Fan, S. F. Liu, *J. Mater, Chem. A* **2015**, *3*, 10693.
[21] C. Ahn, Y. Park, S. Shin, J.-G. Ahn, I. Song, Y. An, J. Jung, C. S. Kim, J. H. Kim, J. Bang, D. Kim, J. Baik, H. Lim, *ACS Appl. Mater. Interfaces* **2021**, *13*, 6805.
[22] J. H. Kim, C. Ahn, J.-G. Ahn, Y. Park, S. Kim, D. Kim, J. Baik, J. Jung, H. Lim, *Appl. Surf. Sci.* **2022**, *587*, 152829.
[23] Y.-C. Lin, W. Zhang, J.-K. Huang, K.-K. Liu, Y.-H. Lee, C.-T. Liang, C.-W. Chu, L.-J. Li, *Nanoscale* **2012**, *4*, 6637.
[24] B. Li, L. Jiang, X. Li, P. Ran, P. Zuo, A. Wang, L. Qu, Y. Zhao, Z. Cheng, Y. Lu, *Sci. Rep.* **2017**, *7*, 1.

How to cite this article: C. Ahn, H. Lim, *Bull. Korean Chem. Soc.* **2022**, *43*(10), 1184. https://doi.org/10.1002/bkcs.12608